Strain-Induced Gap Modification in Black Phosphorus

A. S. Rodin,[1] A. Carvalho,[2] and A. H. Castro Neto[1,2]
[1]Boston University, 590 Commonwealth Avenue, Boston, Massachusetts 02215, USA
[2]Graphene Research Centre and Department of Physics, National University of Singapore, Singapore 117542, Singapore
(Received 5 January 2014; published 1 May 2014)

The band structure of single-layer black phosphorus and the effect of strain are predicted using density functional theory and tight-binding models. Having determined the localized orbital composition of the individual bands from first principles, we use the system symmetry to write down the effective low-energy Hamiltonian at the Γ point. From numerical calculations and arguments based on the crystal structure of the material, we show that the deformation in the direction normal to the plane can be used to change the gap size and induce a semiconductor-metal transition.

DOI: 10.1103/PhysRevLett.112.176801 PACS numbers: 73.20.At, 73.61.Cw

Introduction.—Despite the fact that the variety of truly two-dimensional (2D) materials has been increasing rapidly in recent years [1–3], graphene is set apart from the rest because it contains a single nonmetal atom type. In fact, the choices for such monotypic systems composed of light nonmetals are limited. Carbon is the only solid nonmetal in the second period of the periodic table. The third period contains two such elements: phosphorus and sulfur. Phosphorus is a pnictogen and, as such, typically forms three bonds. This means that it is possible to generate a plane of phosphorus atoms, where every atom has three neighbors. Indeed, there exists a phosphorus allotrope, known as black phosphorus, in which atoms form two-dimensional layers. The layers are held together by weak van der Waals force, similarly to graphite. This allows few-layer black phosphorus structures to be fabricated [4,5]. There are two main traits that set black phosphorus apart from graphite. First, since P atoms are substantially heavier than C atoms, one expects that spin-orbit interaction in phosphorus materials will be stronger. On the structural side, unlike in graphene, the layers are not perfectly flat; instead, they form a puckered surface due to the sp^3 hybridization.

Previous work dealing with black phosphorus monolayers focused on obtaining the band structure using extended tight-binding modeling [6] and *ab initio* calculations [7]. Recently, new studies have appeared dealing with the mobility, band structure, and device fabrication [4,5,8]. The exciting results detailed in these papers illustrate a great potential for practical applications of this material. In this work, we employ the first principles calculation in order to construct an effective low-energy Hamiltonian. Further, we show that uniaxial stress along the direction perpendicular to the layer can be used to change the gap size in the system, transforming the material into a 2D metal.

Structure.—We begin our discussion by looking at the structure of black phosphorus. As a start, it is helpful to consider the best-known phosphorus allotrope: white phosphorus. It is described by the molecular formula P_4. The atoms in the molecule form a tetrahedron with six single bonds so that every P atom has three bonds with its neighbors. From the valence shell electron pair repulsion theory, one can determine that each atom also has a single lone pair. Three bonds and a lone pair result in the sp^3 hybridization of the $3s$ and $3p$ atomic orbitals. Typically, for such a hybridization, bonds and lone pairs stemming from an atom form angles of about 109.5°. However, because of the molecular structure of P_4, the angles between the bonds are 60°. This small angle results in a strain that gives rise to the well-known instability of white phosphorus [9].

Subjecting white phosphorus to high pressure yields black phosphorus. In this case, three out of six bonds in P_4 become broken, resulting in a "tripod"-like shape. Because of the bond breaking, the angles between the remaining bonds become larger, making black phosphorus the most stable allotrope of the element. These flattened P_4 blocks form the black phosphorus layer by having their single-bonded atoms link up with two atoms from other blocks. Despite the partial flattening of the four-atom P clusters, they still retain the sp^3 hybridization character of tetraphosphorus. Because of this, when linked together, the clusters do not form a flat layer and instead result in a puckered structure; see Fig. 1. The illustration shows that the layer is composed of two different orientations of flattened P_4 structures, denoted by the two colors. These two orientations are related by a 180° rotation around the y axis, which runs parallel to the direction of puckering steps. A single buckle is made up of alternating P_4 components. The rest of the lattice is generated by replicating these single steps in the x direction.

The hybridization in black phosphorus results in orbitals that are composed of s and p components. In addition, the puckering breaks the reflection symmetry in the z and x directions. This means that black phosphorus is described by the nonsymmorphic $D_{2h}(7)$ group with the principal axis running along the puckering steps. Without glide planes

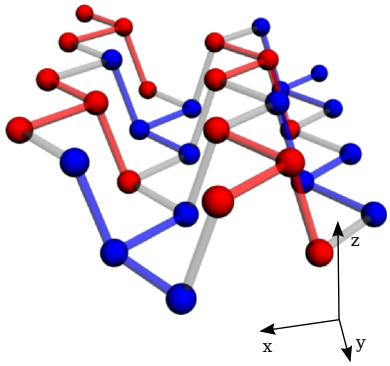

FIG. 1 (color online). P-black monolayer lattice structure in three dimensions. The colors represent two different orientations of the flattened P_4 clusters forming the layer. All bonds are identical, and the colors are used only as a guide to make the symmetry more apparent.

and screw axes, the monolayer symmetry is described by the C_{2h} point group. We will use its irreducible representations later to construct the low-energy Hamiltonian. Finally, also because of the puckering, a unit cell now contains four atoms: C^T, D^T, C^B, D^B (see Fig. 2). Here, C and D denote the sublattice; T and B label the top and bottom of the steps.

First principles calculation.—We use first principles calculations based on density-functional theory (DFT) to obtain the band structure of monolayer black phosphorus. These were performed using the QUANTUM ESPRESSO code [10]. The core electrons were treated using the projector augmented wave method [11]. The exchange correlation energy was described by the generalized gradient approximation (GGA) using the PBEsol functional [12]. Since the order of the conduction bands is very sensitive to strain, this functional was chosen to obtain the accurate structural parameters [13]. The Kohn-Sham orbitals were expanded in a plane-wave basis with a cutoff energy of 70 Ry. The Brillouin zone (BZ) was sampled using 10×8 points following the scheme proposed by Monkhorst-Pack [14].

Black phosphorus monolayer is a direct band gap or nearly direct band gap semiconductor (Fig. 3). The bottom

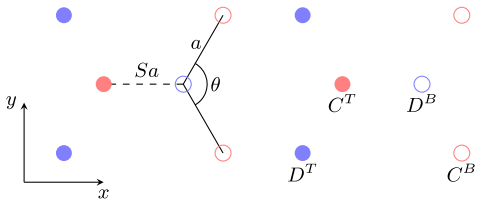

FIG. 2 (color online). Projection of the P-black lattice onto x-y plane. Filled circles correspond to atoms at the top of the buckles, and empty circles are at the bottom. Different colors represent different sublattices. Solid lines are in-plane bonds; the dashed one is out of plane. The length of in-plane bonds is a, and the length of the projection of the out-of-plane ones onto the plane is Sa.

of the conduction band is at Γ (Fig. 3). The valence band top is also close to the Γ point, and it is nearly dispersionless along the y direction. The first principles calculations place its maximum less than $0.06 \times 2\pi/a_y$ away from Γ, where a_y is the lattice parameter along the y direction (see the Supplemental Material [13]). The band gap energy obtained by density functional theory at the GGA level is 0.7 eV.

Similar to the bulk material, the top of the valence band has predominantly p_z character whereas the lowest conduction bands at Γ have mixed p_x and p_z character. The conduction band that increases in energy in the direction X to Γ, i.e., the fourth lowest unoccupied band, has p_y character. All those four conduction bands are very close in energy, and as discussed in the Supplemental Material [13], their relative energy order is very sensitive to deformation along the x direction.

Low-energy Hamiltonian.—Having obtained the band structure using *ab initio* calculations, we now construct a simplified model that describes the bands around the Γ point. Since the valence band maximum is very close to Γ both in the reciprocal space and in energy, we assume the approximation that the band gap is direct. To construct the model, we employ the $\mathbf{k} \cdot \mathbf{p}$ approximation. In this case, the perturbing Hamiltonian is given by $H_1 = \hbar(k_x \hat{p}_x + k_y \hat{p}_y)/m_e$. The true eigenstates of the system at the Γ point are either even or odd with respect to σ_h reflection and can written as sums over irreducible representations of the C_{2h} point group

$$|\Psi_i^e\rangle = |A_g^i\rangle + |B_u^i\rangle, \qquad |\Psi_i^o\rangle = |A_u^i\rangle + |B_g^i\rangle, \quad (1)$$

where $A_{u/g}$ and $B_{u/g}$ are the irreducible representations. Using the symmetry argument, we show how the different bands mix through the perturbing Hamiltonian by rewriting the matrix element $\langle \Psi_i^s | \hat{p}_{x/y} | \Psi_j^{s'} \rangle$ as

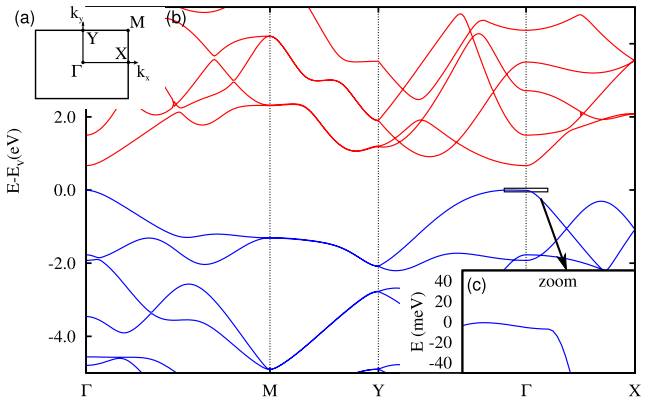

FIG. 3 (color online). First principles band structure of monolayer black phosphorus: (a) diagram identifying the high symmetry points of the Brillouin zone, (b) PBEsol band structure, and (c) detail of the band structure near the Γ point.

$$\langle \Psi_i^s | \sigma_h^\dagger \sigma_h \hat{p}_{x/y} \sigma_h^\dagger \sigma_h | \Psi_j^{s'} \rangle = \pm s s' \langle \Psi_i^s | \hat{p}_{x/y} | \Psi_j^{s'} \rangle, \quad (2)$$

where s, $s' = \pm 1$ are the σ_h symmetry indices. This result tells us that the matrix element for $\hat{p}_x$ ($\hat{p}_y$) is nonzero only if the states have the same (different) σ_h symmetry.

According to the first principles calculations, the valence and the conduction bands are even in σ_h. Thus, to the lowest order, the effective low-energy Hamiltonian is

$$H_{\text{eff}}^0 = \begin{pmatrix} E_c & \gamma_1 k_x \\ \gamma_1^* k_x & E_v \end{pmatrix}, \quad (3)$$

where $\gamma_1 = \hbar \langle \Psi_c | \hat{p}_x | \Psi_v \rangle / m_e$. Note that without including the rest of the bands, Eq. (3) describes a one-dimensional system. The lack of y dependence agrees with the weak dispersion in the y direction close to the Γ point seen in the numerical results. The rest of the H_{eff} is obtained by including the remaining bands and using the Löwdin partitioning [15]. The leading order correction to the effective Hamiltonian is given by

$$(H_{\text{corr}})_{mm'} = \sum_l \frac{(H_1)_{ml}(H_1)_{lm'}}{2} \left[\frac{1}{E_m - E_l} + \frac{1}{E_{m'} - E_l} \right], \quad (4)$$

where the summation goes over the remaining bands. The diagonal elements of the correction are

$$(H_{\text{corr}})_{mm} = \sum_l \frac{(\gamma_{ml}^x)^2 k_x^2 + (\gamma_{ml}^y)^2 k_y^2}{E_m - E_l} = \eta_m k_x^2 + \nu_m k_y^2. \quad (5)$$

This result captures the mass difference between the conduction and the valence bands as well as the $\hat{x}$ and $\hat{y}$ directions.

Finally, the off-diagonal elements are

$$(H_{\text{corr}})_{cv} = \alpha k_x^2 + \beta k_y^2, \quad (6)$$

$$\alpha = \sum_{l,\text{even } \sigma_h} \frac{\gamma_{cl}^x \gamma_{vl}^x}{2} \left[\frac{1}{E_c - E_l} + \frac{1}{E_v - E_l} \right], \quad (7)$$

$$\beta = \sum_{l,\text{odd } \sigma_h} \frac{\gamma_{cl}^y \gamma_{vl}^y}{2} \left[\frac{1}{E_c - E_l} + \frac{1}{E_v - E_l} \right], \quad (8)$$

resulting in

$$H_{\text{eff}} = \begin{pmatrix} E_c + \eta_c k_x^2 + \nu_c k_y^2 \gamma_1 k_x + \alpha k_x^2 + \beta k_y^2 \\ \gamma_1^* k_x + \alpha k_x^2 + \beta k_y^2 E_v + \eta_v k_x^2 + \nu_v k_y^2 \end{pmatrix}. \quad (9)$$

From this, one can obtain the effective masses close to the Γ point

$$m_{c/v}^x = \frac{\hbar^2}{2\left(\pm \frac{|\gamma_1|^2}{\Delta} + \eta_{c/v} \right)}, \qquad m_{c/v}^y = \frac{\hbar^2}{2\nu_{c/v}}. \quad (10)$$

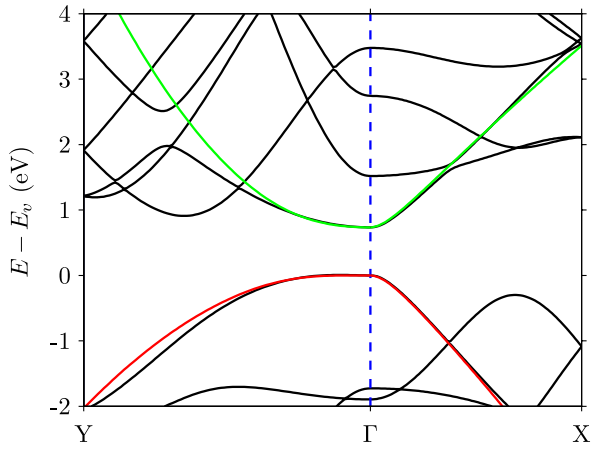

FIG. 4 (color online). Fitting of the H_{eff} results to the *ab initio* band structure. For this fit, $\gamma_1 = 6.85w/\pi$ eV m, $\eta_v = -3w^2/\pi^2$ eV m^2, $\nu_c = 5w^2/\pi^2$ eV m^2, and $\beta = 7w^2/\pi^2$ eV m^2, where $w \approx 2.23 \times 10^{-10}$ m and π/w is the BZ width in the $\hat{x}$ direction. The rest of the parameters are set to zero. Note that this fit gives a direct gap.

Close to the Γ point, we retain only the leading coupling terms and set $\alpha = 0$. We plot a fit for the conduction and valence bands in Fig. 4.

Lattice deformation.—Application of uniaxial stress in the direction perpendicular to the monolayer modifies the band structure. It is known that the symmetry breaking in general lifts degeneracies and opens gaps. In this system, however, vertical compression does not break symmetry. Rather, as the thickness decreases, the system moves towards the more symmetric state where the T and B subsystems become identical. This will result in the change of the gap size and, for compressive strain, induce a semiconductor-metal transition.

We show in the Supplemental Material [13] that at the Γ point the Hamiltonian can be separated into four families

$$H_{nm} = \Sigma + nPZ + m[M + nK_C Z]L. \quad (11)$$

Σ is the on-site energy matrix, P is the hopping matrix between T and B subsystems of the same sublattice (C and D), M describes hopping between C_T and D^T, and K_C connects C^T to D^B. Z is a diagonal matrix with $(1, 1, 1, -1)$, and L is a diagonal matrix with $(-1, 1, 1, 1)$. Finally, $m, n = \pm 1$. States with $m = 1$ are antisymmetric in s orbitals for atoms on the same level (T and B) and symmetric in other orbitals. For $n = 1$, the T and B atoms of the same sublattice are symmetric in s, p_x, and p_y and antisymmetric in p_z.

To understand how the deformation affects the gap size, it is helpful to consider two limiting cases: a completely flattened layer and a layer where the bonds connecting T and B subsystems are perpendicular to them (maximum puckering). In the first case, p_z orbitals become orthogonal

to the rest. In addition, T/B symmetry is restored and $n = -1$, yielding the following energies at the Γ point

$$E_{\text{flat}} = \Sigma_z + mM_z. \tag{12}$$

Σ_z is the energy arising from the overlap of the single sublattice (C or D) p_z orbitals, and M_z is the sum over all the π bonds between the sublattices. Since the hopping element for π bonds is negative, $M_z < 0$. This means that the state where all the p_z orbitals are aligned in the same direction have the energy $E = \Sigma_z + M_z$, smaller than the state where the sublattices are antisymmetric in p_z ($E = \Sigma_z - M_z$). The reason for this is that the symmetric arrangements results in bonding, which is lower in energy than the antibonding antisymmetric arrangement. As will be shown below, flattening leads to an in-plane lattice deformation, and the monolayer approaches a square lattice. This, however, does not change our argument as the parallel arrangement of p_z orbitals is still lower in energy compared to the antiparallel one.

Let us now move on to the maximum-puckering case. Here, neighboring $C^{T/B}$-$D^{B/T}$ atoms are aligned along the $\hat{z}$ axis. This means that symmetrically aligned neighboring p_z orbitals form an antibonding σ bond instead of the bonding π bond. Similarly, antisymmetric neighbors form a σ bond instead of the π antibond. In fact, the general nature of $C^{T/B}$-$D^{B/T}$ interaction becomes more bonding for the antisymmetric case and more antibonding for the symmetric case as one goes from a flat to a puckered system. If the σ bond energy is substantially larger than that of the π bond, puckering can actually cause the previously antibonding arrangement to become bonding and vice versa. In fact, according to our numerical calculations, the lowest conduction band is described by $H_{-1,-1}$, see Eq. (11), corresponding to the fully symmetric p_z orientation. On the other hand, the highest valence band has $n = -1$, $m = 1$, which is antisymmetric. Clearly, the ordering of the bands is opposite to what one finds in a flat layer. This means that layer compression leads to the gap reduction and an eventual band crossing.

To confirm this conclusion, we modeled the strained layers using density functional theory. The monolayer unit cell and atomic positions were relaxed subject to the constraint $z = \pm h$ for all atoms. Compression ($h < h_0$, where $2h_0$ is the thickness of the free layer) results in an in-plane expansion of the unit cell. Until $h/h_0 \sim 0.4$, the bonding structure of black phosphorus remains, and the structure of the strained material approaches that of a puckered graphene layer [Figs. 5(a) and 5(b)]. Below $h/h_0 \sim 0.2$, however, there is a transformation into a square lattice [Fig. 5(c)].

With regard to the band structure, the valley at Γ, marked A in Fig. 5(a), first raises while the valley B becomes lower in energy. Hence, at $h/h_0 = 0.94$, the material is an indirect-gap semiconductor. With further compression, a new valley appears at the Y point [marked C in Fig. 5(b)]. For $h/h_0 \sim 0.75$, this one eventually becomes as low as the valence band top near Γ, marking the transition from indirect band gap semiconductor to metallic. Figure 5(d) shows the variation of the band gap energy, until a point where the conduction band minimum has descended below the valence band maximum. The uniaxial stress that is necessary to impose in order to achieve the semiconductor to metal transition is estimated to be about 24 GPa, from the Hellman-Feynman forces [10].

In a narrow range of h/h_0 between 0.75 and 0.70, the material has a low density of states at the Fermi level and can be considered a semimetal. If compression is increased, the original valence bands and conduction bands finally cross.

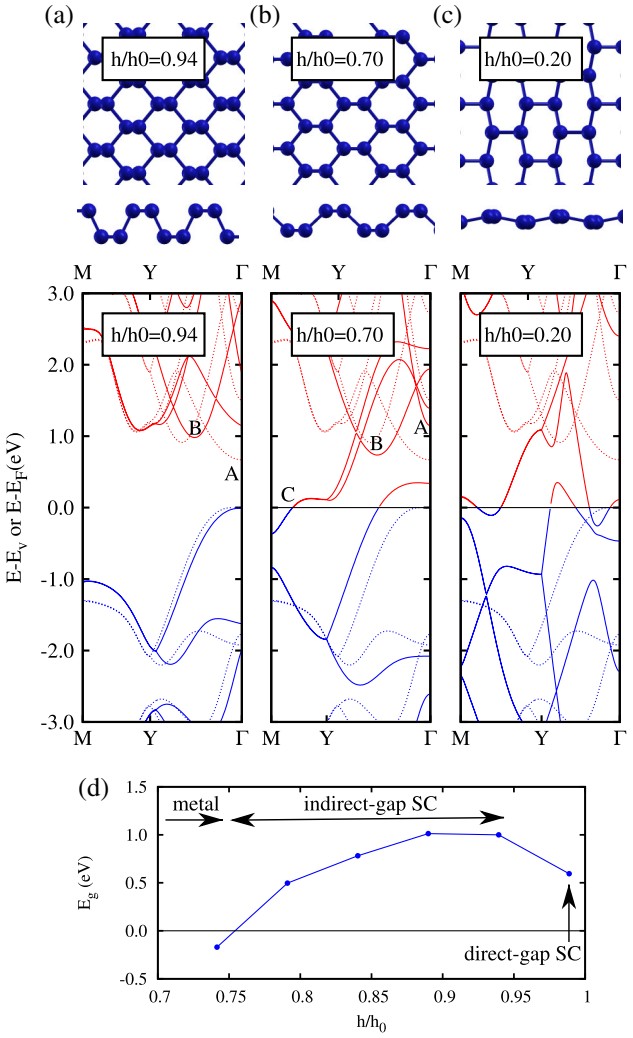

FIG. 5 (color online). [(a)—(c)] Band structure of black phosphorus monolayer under uniaxial compression along the z direction, for three values of the imposed height h/h_0 (continuous line), along with the band structure of the pristine material (dotted lines). The respective relaxed structure is also depicted in top and side views. (d) Band gap as a function of the height. The original layer thickness is $2h_0$.

Below $h/h_0 \sim 0.2$ where the lattice is already nearly square, the resemblance of the bands to those of the original material is completely lost [Fig. 5(c)].

Conclusions.—Using *ab initio* calculations, we have obtained the band structure of single-layer black phosphorus. The results show that this material is a direct band gap or nearly direct band gap semiconductor with a strongly anisotropic dispersion in the vicinity of the gap. From the first principles calculation, we also obtain the localized orbital composition of the bands around the Γ point, which allows us to construct an effective Hamiltonian that describes the highest valence and the lowest conduction bands.

On the basis of the lattice structure of black phosphorus, we use a general tight-binding description to predict the closing of the gap with compression in the transverse direction. To support this prediction, we use DFT to show that upon moderate deformation, the system goes through a semiconductor-metal transition. The energy ordering of the conduction band valleys changes with strain in such a way that it is possible to switch from nearly direct band gap semiconductor to indirect semiconductor, semimetal, and metal with the compression along *only one direction*. Finally, under severe compression, the monolayer approaches a plane square lattice configuration. Such rich variety of electronic and structural transformations makes P-black a unique material for fundamental physics studies.

A. S. R. acknowledges DOE Grant No. DE-FG02-08ER46512 and ONR Grant No. MURI N00014-09-1-1063. A. H. C. N. acknowledges NRF-CRP Grant "Novel 2D materials with tailored properties: beyond graphene" (No. R-144-000-295-281). The first principles calculations were carried out on the GRC high-performance computing facilities.

[1] N. Alem, R. Erni, C. Kisielowski, M. D. Rossell, W. Gannett, and A. Zettl, Phys. Rev. B **80**, 155425 (2009).
[2] B. Lalmi, H. Oughaddou, H. Enriquez, A. Kara, S. Vizzini, B. Ealet, and B. Aufray, Appl. Phys. Lett. **97**, 223109 (2010).
[3] Q. H. Wang, K. Kalantar-Zadeh, A. Kis, J. N. Coleman, and M. S. Strano, Nat. Nanotechnol. **7**, 699 (2012).
[4] H. Liu, A. T. Neal, Z. Zhu, D. Tománek, and P. D. Ye, arXiv:1401.4133.
[5] L. Li, Y. Yu, G. J. Ye, Q. Ge, X. Ou, H. Wu, D. Feng, X. H. Chen, and Y. Zhang, arXiv:1401.4117.
[6] Y. Takao and A. Morita, Physica B+C (Amsterdam) **105**, 93 (1981).
[7] Y. Du, C. Ouyang, S. Shi, and M. Lei, J. Appl. Phys. **107**, 093718 (2010).
[8] J. Qiao, X. Kong, Z.-X. Hu, F. Yang, and W. Ji, arXiv:1401.5045.
[9] N. N. Greenwood and A. Earnshaw, *Chemistry of the Elements* (Butterworth Heinemann, Oxford, 1998).
[10] P. Giannozzi *et al.*, J. Phys. Condens. Matter **21**, 395502 (2009).
[11] P. E. Blöchl, Phys. Rev. B **50**, 17953 (1994).
[12] J. P. Perdew, A. Ruzsinszky, G. I. Csonka, O. A. Vydrov, G. E. Scuseria, L. A. Constantin, X. Zhou, and K. Burke, Phys. Rev. Lett. **100**, 136406 (2008).
[13] See the Supplemental Material at http://link.aps.org/supplemental/10.1103/PhysRevLett.112.176801 for details, which includes Refs. [16–27].
[14] H. J. Monkhorst and J. D. Pack, Phys. Rev. B **13**, 5188 (1976).
[15] R. Winkler, *Spin-Orbit Coupling Effects in Two-Dimensional Electron and Hole Systems* (Springer-Verlag, Berlin, Heidelberg, 2003).
[16] Ø. Prytz and E. Flage-Larsen, J. Phys. Condens. Matter **22**, 015502 (2010).
[17] J. P. Perdew and Y. Wang, Phys. Rev. B **45**, 13244 (1992).
[18] J. P. Perdew, K. Burke and M. Ernzerhof, Phys. Rev. Lett. **77**, 3865 (1996).
[19] J. Heyd, G. E. Scuseria, and M. Ernzerhof, J. Chem. Phys. **118**, 8207 (2003).
[20] K. Lee, E. D. Murray, L. Kong, B. I. Lundqvist, and D. C. Langreth, Phys. Rev. B **82**, 081101 (2010).
[21] L. Cartz, S. R. Srinivasa, R. J. Riedner, J. D. Jorgensen, and T. G. Worlton, J. Chem. Phys. **71**, 1718 (1979).
[22] D. Sánchez-Portal, P. Ordejón, E. Artacho, and J. M. Soler, Int. J. Quantum Chem. **65**, 453 (1997).
[23] E. Artacho, D. Sánchez-Portal, P. Ordejón, A. García, and J. M. Soler, Phys. Status Solidi B **215**, 809 (1999).
[24] O. F. Sankey and D. J. Niklewski, Phys. Rev. B **40**, 3979 (1989).
[25] O. F. Sankey, D. J. Niklewski, D. A. Drabold, and J. D. Dow, Phys. Rev. B **41**, 12750 (1990).
[26] N. Troullier and J. L. Martins, Phys. Rev. B **43**, 1993 (1991).
[27] L. Kleinman and D. M. Bylander, Phys. Rev. Lett. **48**, 1425 (1982).